FEA Based on 3D Micro-CT Images of Mesoporous Engineered Hydrogels

L. Siad
University of Champagne, France
larbi.siad@univ-reims.fr

J. Jing
University of Champagne, France
jing.jing@univ-reims.fr

J. Braux
University of Champagne, France
Julien.braux@univ-reims.fr

M. Dubus
University of Champagne, France
marie.dubus@univ-reims.fr

F. Velard
University of Champagne, France
frederic.velard@univ-reims.fr

D. Laurent-Maquin
University of Champagne, France
dominique.laurent-maquin@univ-reims.fr

S. C. Gangloff
University of Champagne, France
sophie.gangloff@univ-reims.fr

H. Kerdjoudj
University of Champagne, France
halima.kerdjoudi@univ-reims.fr

R. Rahouadj
University of Lorraine, France
rachid.rahouadj@univ-lorraine.fr

J. -F. Schmidt
University of Lorraine, France
jean-francois.schmidt@univ-lorraine.fr

J. -F. Ganghoffer
University of Lorraine, France
jean-francois.ganghoffer@univ-lorraine.fr

***Abstract* —The objective of this computational study was to propose a rapid procedure in obtaining an estimation of elastic moduli of solid phases of porous natural-polymeric biomaterials used for bone tissue engineering. This procedure was based on the comparison of experimental results to finite element (FE) responses of parallelepiped so-called representative volume elements (rev) of the material at hand. To address this issue a series of quasi-static unconfined compression tests were designed and performed on three prepared cylindrical biopolymer samples. Subsequently, a computed tomography scan was performed on fabricated specimens and two 3D images were reconstructed. Various parallelepiped revs of different sizes and located at distinct places within both constructs were isolated and then analyzed under unconfined compressive loads using FE modelling. In this preliminary study, for the sake of simplicity, the dried biopolymer solid is assumed to be linear elastic.**

Keywords-Porous biomaterials; finite element; micro-CT; elasticity.

I. INTRODUCTION

Polysaccharides fall into the category of biopolymers derived from natural sources; their properties make them suitable for various biomedical and pharmaceutical applications [28, 37] including, e.g., tissue engineering purposes. The success of polysaccharides like chitosan for these applications stems from the fact that they are natural, abundant, and renewable polymers (originate from, e.g., algae and plants). Furthermore, they are biocompatible and biodegradable [22, 38]. In addition, polysaccharides are characterized by a wide variety of structures that lead to peculiar properties that can hardly be matched, if necessary, by synthetic materials.

On the other hand, considerable attention has been focused on microcomputed tomography (micro-CT), a non-destructive technique, which yields 3D information of the material analyzed through high-fidelity models constructed from data images. Besides, nowadays image-based meshing offers interesting opportunities based on microstructures scan data to computational continuum micromechanics methods for material characterization [7, 25, 27]. This approach turns out to be very attractive in materials science where the link between macroscopic properties and the micro-structure of a material is sought.

II. POLYMERIC GELS - A BRIEF OVERVIEW

Polymeric gels consist of physically or chemically cross-linked polymer chains that are able to absorb large amounts of solvent molecules (for instance, biological fluid) without dissolving [11, 16, 26, 29, 31]. They are called hydrogels when the solvent is water. Hydrogels have the capability to mimic the extracellular matrix and their soft nature matches that of biological tissues. Subsequently, they are hence highly desirable as 3D scaffolds for cells encapsulation [2]. Based on the bonding type of the crosslinks, polymeric gels are classified into chemical gels (covalent bonds) or physical gels (cohesion forces existing between polymer segments, e.g., ionic bonding, van der Waals forces …). The strong chemical bonds enable the polymeric gel to keep its shape after a large deformation. The high solvent content and elasticity yield a resemblance to biological tissue, creating extensive biomedical applications. At the same time, many tissues consist of elastic network and mobile molecules; the elasticity enables the tissues to retain shapes and deform, while mobile molecules enable the tissues to transport nutrients and wastes [18, 19, 20, 36].

The deformation of polymeric gels (swelling) can be affected by many external factors (stimuli) like forces, temperature, electrical or magnetic fields, pH values, ionic concentration, many other types of stimuli. Their response to these stimuli is generally a transient process involving solvent diffusion and deformation coupled via the chemo-mechanical interactions of polymer network and present solvent. Such stimuli-responsive gels have become a good material choice in numerous applications. Among them one could specifically name scaffolds for tissue engineering, drug delivery applications, and model of ECM for biological studies. It is believed that precisely because polymeric gels are responsive to various types of stimuli due to different mechanisms, a unified constitutive model that covers all of them seems to be very tedious to construct. Generally speaking, the three main components of the polymeric gels synthesis are monomers, initiator, and crosslinkers which have good solubility in solvent at hand [11, 16, 23, 26]. Nowadays, it is possible to design the structure of polymeric gels for a specific application by selecting proper starting materials and processing techniques. Indeed, more and more polymeric gels have been engineered with tunable microstructures, mechanical properties, and also degradable rates.

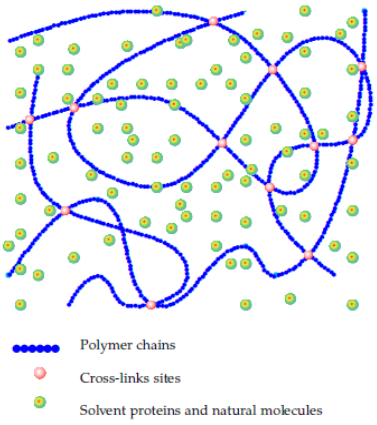

Fig. 1. The 3d structure of a covalently cross-linked polymeric gel is a result of polymer cross-linking that forms an insoluble structure within the fluid environment where the network of polymer chains swell.

Constitutive models based on deformation, chemical diffusion, and transformation mechanisms of the chemical and mechanical energy of polymeric gels are receiving more and more attention. The thermodynamics of swelling dates at least back to Gibbs [6] who formulated an equilibrium theory for the deformation of an elastic solid that absorbs a fluid. Biot [15] used thermodynamic theory and Darcy's law to model the mass transport in a porous solid. As a matter of fact, these early works were not specific for polymeric gels. Flory and Rehner [12, 13] and Flory [14] developed a statistical-mechanical model for gels. Based on these seminal works, continuum models accounting for, amongst others, chemically induced volume transition, diffusion of a fluid, and inhomogeneous swelling in elastomeric gels are formulated and analyzed in [4, 5, 8, 10, 19, 20]. Suo, Hong and their coworkers [18, 19, 20, 36] modified the Flory-Rehner model for neutral gel by adopting the interaction parameter as a function of temperature and concentration.

With a specific material model, such a theory enables analysis for the deformation of temperature-responsive polymeric gel under different geometric and mechanic constraints. As a model material, the polymeric gel is characterized by a Helmholtz free-energy density function proposed by Flory and others. This free-energy function accounts for, at the very last, the stretching of the polymer network and mixing of the polymer network and the solution. Indeed, in neutral (as opposed to ionic) polymeric gels, there are two competing energies within the system. The energy that resists the solvent migration comes from the entropy of stretching the polymer chains and the energy that drives the influx of solvent is from the entropy of mixing. When solvent molecules migrate into a neutral polymeric gel, the possible arrangements of the system increase, leading to greater entropy of the mixture compared with the separated components, [16, 19, 20]. The interaction between the polymer network and solvent results in the heating of the mix.

If the density of the crosslinks is very low, the effect of crosslinks on mixing can be reasonably neglected. In this circumstance, it is reasonable to assume that the free-energy density function of the polymeric gel is simply written as the sum $W = W_{stretch} + W_{mix}$, where $W_{stretch}$ and W_{mix} are the contributions from stretching the polymer network and mixing the polymers network and the solvent, respectively, [12, 13, 14]. This model (classical) is still being widely used to describe various approximate behaviours of polymeric gels.

In order to trace the deformation of the polymeric gel, the dried polymer network under no mechanical load is taken as the reference state. Each marker is named by its coordinate X in the reference state. In the current state at time *t*, the marker X moves to a place with coordinate $x(X,t)$. The local stretching state of the polymer network near marker X can be described by the deformation gradient $F(X,t)$. In addition, the solvent molecules constantly change their neighbors and migrate freely in and out of the polymeric gel. To account for the mobile species, we define the field of nominal solvent concentration $C(X,t)$, so that $C\,dV$ is the number of solvent molecules in a volume element in the current state. For neutral one species of polymer chains and one species of solvent molecules, both being electroneutral polymeric gel, the two commonly used field variables are the deformation gradient and the nominal solvent concentration, in situations of isothermal processes (the temperature is deleted from the list of state variables): $W = W(F,C)$. The free energy of a surface or interface is disregarded. A simple form of the Helmholtz free-energy density function is

$$W(F,C) = W_{stretch}(F,C) + W_{mix}(C) \qquad (1)$$

The scope of polymeric gels applications is often severely limited by their mechanical properties, in particular their low elastic moduli. In the current paper, we limit our investigation to small deformation and to the linear elastic response of the

dried polymer network ($C = 0$). As a result, the strain energy density function of stretching the dried polymer network, in terms of infinitesimal strain tensor ε, is

$$W(\varepsilon_{ij}) = \frac{1}{2}\left(\frac{\nu E}{(1+\nu)(1-2\nu)} \varepsilon_{kk}^2 + \frac{\nu E}{(1+2\nu)} \varepsilon_{ij}\, \varepsilon_{ij} \right) \qquad (2)$$

where E is the Young's modulus and ν is the Poisson's ratio of the material at hand. This is the St. Venant-Kirchhoff model which is the simplest example of a hyperelastic material. It should be kept in mind that this St. Venant-Kirchhoff material has been found to be of little practical use beyond the small strain domain.

III. UNIAXIAL COMPRESSION TESTS

Three-dimensional mesoporous scaffolds have been manufactured according to the freeze-drying procedure. For a detailed description of the used process allowing the preparation of the mesoporous polymeric biomaterial, we refer the reader to the paper by Brun et al. [3]. The porosity of the investigated cylindrical samples, measured by the liquid displacement method, was estimated to range from 80 to 91 % with a pore size of 50 to 150 μm. The uniaxial (or unconfined) compression test is often chosen to characterize porous materials because of the simplicity of the testing configuration and the specimen test shape. A typical compression test involves influence of specimen size, influence of porosity, and strain rates effects on mechanical response of the material [9]. Usually compression data including, for example, Young's modulus, yield stress and Poisson's ratio, is obtained from the measured force versus the displacement curve. In this preliminary work, unconfined compression tests were carried out first in order to obtain an appraisal of the Young's modulus E of built scaffolds

Circular cylindrical samples with about 10.0 mm in diameter and 9.0 mm in height were subject to unconfined compression through an universal testing machine at a strain rate of $20\times10^{-3}\ s^{-1}$ (Figure 2). Both chemical crosslinked and uncrosslinked scaffolds were tested. In this paper the focus is only on the former biomaterial for which Figure 3 displays the obtained stress-strain curves due to loading (increasing strain) and unloading (decreasing strain) for three distinct samples. The curves seem to be linear for stresses up to about 100 kPa .

The mean experimental values of Young' moduli of the tested samples were measured as the slopes of linear elastic-unloading curves, using the approximate expression: (Figure 4)

$$E_{exp} \simeq H_o\left(\frac{\Delta\sigma}{\Delta H}\right),\ \Delta\sigma = \sigma^{(2)} - \sigma^{(1)}\ ,\ \Delta H = H^{(2)} - H^{(1)} \quad (3)$$

In this way, for the considered crosslinked scaffold it has been found that $E_{exp} \simeq 19.20$ MPa .

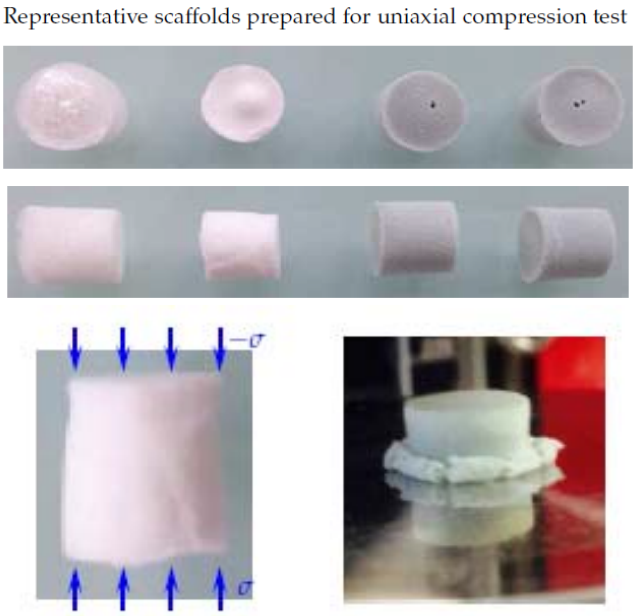

Fig. 2. Prepared crosslinked scaffold for compression tests. a) Uniaxial compression stress state; b) Specimen typical failure mode.

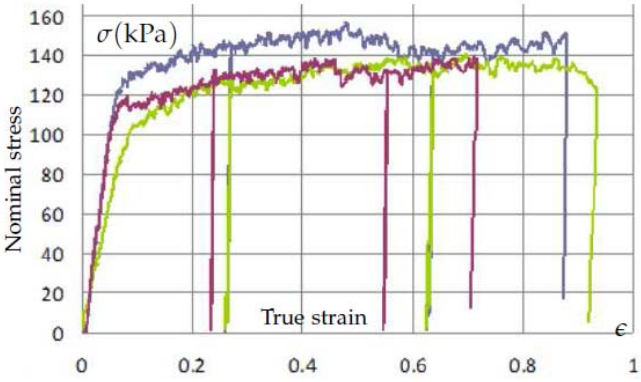

Fig. 3. Nominal stress versus true strain curves for crosslinked scaffolds. The 3 curves correspond to 3 distinct samples.

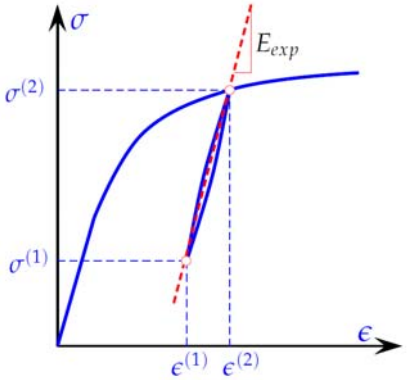

Fig. 4. Used technique for the determination of the mean value of the Young's modulus from experimental results.

IV. FINITE ELEMENT MODELING

High-resolution three-dimensional micro-CT scan data of cylindrical samples were obtained and the data were straightforwardly segmented using threshold and flood fill tools in Simpleware's ScanIP software [35]. The pixel size was 8.85 μm. The 3D connectivity of the dried biopolymer turns out to be practically totally interconnected (Figure 2). As a trade-off, various parallelepiped specimens having the same cross section A_o (0.345 × 0.345, 0.522 × 0.522, 0.699 × 0.699 and 0.965 × 0.965 mm^2) with increasing thickness H_o (0.345, 0.531, 0.708 and 0.965 mm) were used in this preliminary investigation. They were extracted from the 3D image as shown in Figure 5.

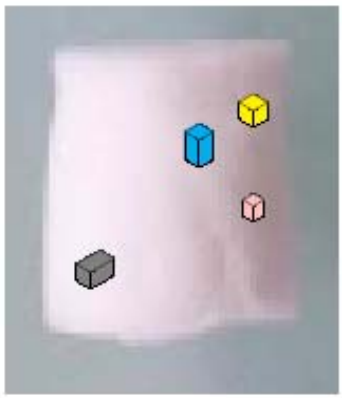

Fig. 5. Various parallelepiped **rve**s for uniaxial compression simulations. Typical example of rve size: 60×89×60 voxels; one pixel = 8.85 µm.

The corresponding 3D micro-CT image data are converted into FE models. The parallelepiped specimens were meshed with the same mesh density. The anti-aliasing techniques implemented in this software are volume, topology and geometry preserving. Mixed hexahedral and tetrahedral elements were generated. The element parameters were adjusted to the software recommended aspect ratio in order to ensure the highest mesh quality possible [35].

The various samples were subject to compression tests along the z-direction. To this goal, a displacement which amplitude depends on the considered sample is imposed on top faces perpendicular to the z-direction, whereas the bottom faces were fixed along z-direction and the four other faces remain free. We made the assumption that the behavior of the solid phase of the considered porous biomaterials remains linear elastic during the whole process of deformation. A series of FE analyses using Abaqus [1] were carried out under compression loading conditions up to approximately 30 % strain. It is believed that this is high enough to observe local deformation. By way of illustration, Figure 6 shows a typical mesh geometry created from tomographic images using Simpleware [35]. Prior to simulation as such, a wide number of analyses were performed in order to get insight of the sensitivity of numerical predictions to mesh density and segmentation parameters. Vertical total reaction force F_z of the top moving face and its vertical displacement u_z were recorded during the simulated compression test. The nominal compression stress σ was calculated as the ratio of F_z on its initial total area A_o : $\sigma = F_z / A_o$. The engineering strain ε is given by $\varepsilon = (H - H_o) / H_o$.

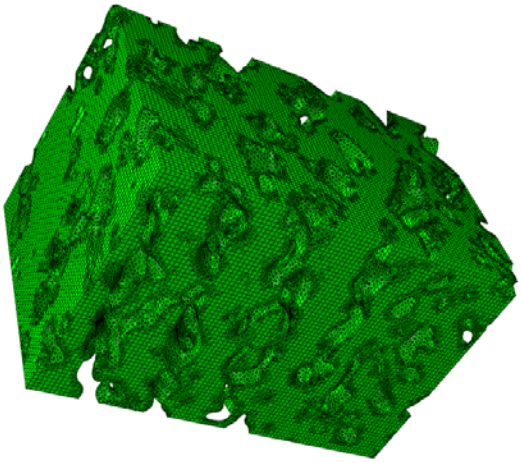

Fig. 6. FE mesh of a parallelepiped created from tomographic images [9]. The FE model includes about 920 940 hexahedral and tetrahedral elements.

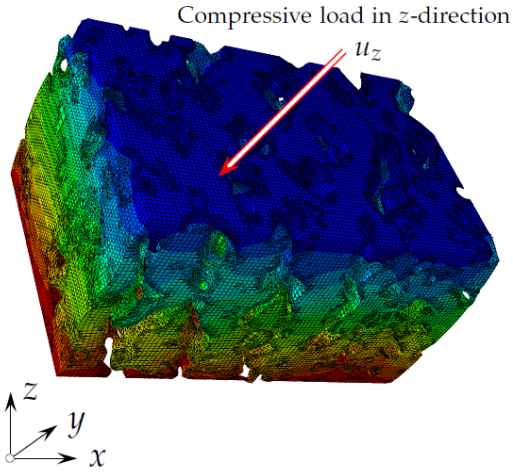

Fig. 7. 3D visualization of the contour plot of the z-displacement.

V. RESULTS AND DISCUSSION

The whole simulated parallelepiped specimens exhibited a similar mechanical trend under compression loading. By way of example, Figure 7 displays a deformed contour plot of the u_z component of the displacement **u** calculated using the procedure described above. As regard our first simulation, the used values of Young's modulus and Poisson's ratio of the porous biomaterials at hand were obtained from a literature review dealing with chitosan, e.g., [23, 32, 38]: $E \simeq 380$ MPa, $\sigma_y \simeq 110$ MPa. It emerged that using these values yields a large overestimation of the Young' moduli in comparison to experimental results.

The foregoing FE modelling is used, thanks to the linearity of the problem under consideration, to obtain an estimation of the Young's modulus of the chemical crosslinked biomaterials which preparation is described in [3]: $E_{pg} \simeq 27.73$ MPa for µ-CT construct sample 1 and $E_{pg} \simeq 45.51$ MPa for µ-CT construct sample 2.

After which these values have used in order to get an estimation of the apparent Young's modulus E_a, for a fixed volume size of considered **rve**s. The obtained results are shown in Table I, Figure 8 and Table II, Figure 9, respectively. One has to notice that when the size of the simulated specimen is smaller than the **rve** of the material, the properties that can be computed are not necessarily the effective properties but merely apparent properties of the investigated volume, [17, 21, 24, 34]. The computer used throughout the present study is a standard PC. Within the context of random heterogeneous materials, it should be kept in mind that larger computer facilities would be necessary in order to analyze specimens with larger sizes.

TABLE I. COMPUTED APPARENT YOUNG'S MODULUS AS A FUNCTION OF THE THICKNESS H_o OF THE SIMULATED RVE; $E_{PG} = 27.73$ MPA.

µCT CONSTRUCT 1				
H_o (µm)	345.2	522.2	699.2	964.7
E_a (MPa)	16.94	17.48	17.81	19.20

µCT CONSTRUCT 2							
H_o (µM)	345.2	345.2	345.2	522.2	522.2	692.2	964.5
E_A (MPA)	15.42	12.99	13.42	15.91	13.26	14.02	13.76

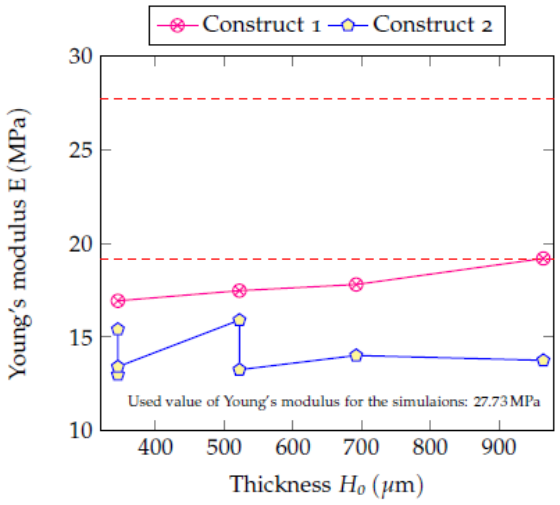

Fig. 8. Computed apparaent Young's modulus E_A as a function of the thickness H_o of the simulated parallelipiped **rve**; $E_{pg} = 27.73$ MPa.

TABLE II. COMPUTED APPARENT YOUNG'S MODULUS AS A FUNCTION OF THE THICKNESS H_o OF THE SIMULATED RV; $E_{PG} = 45.51$ MPA

µCT CONSTRUCT 1				
H_o (µm)	345.2	522.2	699.2	964.7
E_a (MPa)	23.65	24.40	24.86	26.80

µCT CONSTRUCT 2							
H_o (µM)	345.2	345.2	345.2	522.2	522.2	692.2	964.5
E_A (MPA)	18.73	18.14	21.53	18.51	22.22	19.57	19.20

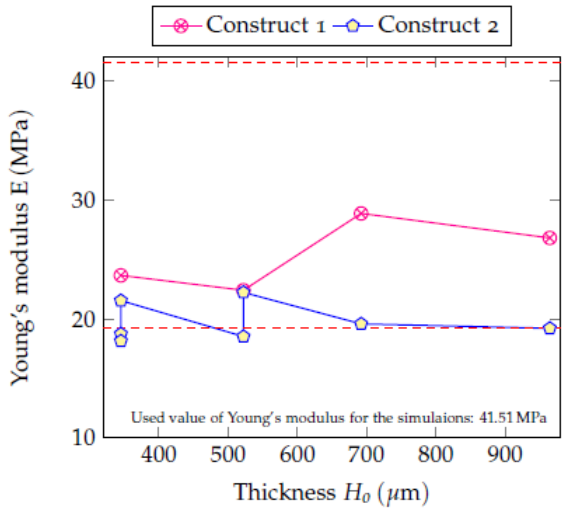

Fig. 9. Computed apparaent Young's modulus E_A as a function of the thickness H_o of the simulated parallelipiped **rve**; $E_{pg} = 45.51$ MPa.

VI. CONCLUSION AND FUTURE PROSPECTS

The foregoing numerical model accounts for the micro architecture of the porous polymeric biomaterials at hand. This and prior work highlights that FE models based on an accurate 3D model from micro-CT data are an essential tool to quantify the effects of pores in complex material systems such as polymeric biomaterials. The ease with which models can be generated would allow us to account for, e.g., the hyperelastic and the viscoelastic behaviour of the materials at hand. These constitutive models can be coupled with FE biomechanical simulations to analyse the behaviour of chitosan-hyaluronic acid based materials used as scaffolds for tissue engineering. These extensions are contemplated as future works.

References

[1] ABAQUS/Standard, SIMULIA, Providence, RI, 2013

[2] E. M. Ahmed, "Hydrogel: Preparation, characterization, and applications: A review", Journal of Advanced Research, Vol. 6, pp. 105-121, 2015

[3] V. Brun, C. Guillaume, S. Mechiche Alami, J. Josse, J. Jing, F. Draux, S. Bouthors, D. Laurent-Maquin, S. C. Gangloff, H. Kerdjoudj, F. Velard, "Chitosan/hydroxyapatite hybrid scaffold for bone tissue engineering", Biomed. Mater. Eng., Vol. 24, pp. 63-73, 2014

[4] S. Baek, A. R. Srinivasa, "Diffusion of a fluid through an elastic solid undergoing large deformation", Int. J. Non-linear Mech., Vol. 39, pp. 201-218, 2004

[5] S. Baek, T. J. Pence, "Inhomogeneous deformation of elastomer gels in equilibrium under saturated and unsaturated conditions", J. Mech. Phys. Solids, Vol. 59, pp. 561-582, 2011

[6] M. A. Biot, "General theory of three-dimensional consolidation", J. Appl. Phys., Vol. 12, pp. 155-164, 1941

[7] S. K. Boyd, "Image-Based Finite Element Analysis" in C. W. Sensen, B. Hallgrimson, editors, Advanced Imaging in Biology and medecine, pp. 3-25, Springer, Berlin, 2009

[8] S. A. Chester, L. Anand, "A coupled theory of fluid permeation and large deformations for elastomeric materials", J. Mech. Phys. Solids, Vol. 58, pp. 1879-1919, 2010

[9] S.C. Cowin, S.B. Doty, Tissue mechanics, Springer, Berlin, 2007.

[10] J. Delbow, E. Fried, H. Ji, "Chemically induced swelling of hydrogels", J. Mech. Phys. Solids, Vol. 52, pp. 51-84, 2004

[11] M. Djabourov, K. Nishinari, E. Schacht, Physical Gels from Biological and Synthetic Polymers, Cambridge University Press, 2013

[12] P. J. Flory, J. Rehner, "Statistical mechanics of cross-linked polymer networks I. Rubberlike elasticity", J. Chem. Phys., Vol. 11, pp. 512-520, 1943

[13] P. J. Flory, J. Rehner, "Statistical mechanics of cross-linked polymer networks II. Swelling", J. Chem. Phys., Vol. 11, pp. 521-526, 1943

[14] P. J. Flory, Principles of Polymer Chemistry, Cornell University Press, Ithaca, 1953

[15] J. W. Gibbs, The Scientific papers of J. Willard Gibbs, Dover Publication, New York, 1961. Digital copy of the book is freely available at http://books.google.com/

[16] F. Horkay, G. B. McKenna, "Polymer network and gels", in J. E. Mark, editor, Physical properties of polymers handbook, pp. 497-523, Springer, Berlin, 2007

[17] S. Hazanov, C. Huet, "Order relationships for BCs effect", J. Mech. Phys. Solids, Vol. 42, pp. 1995–2011, 1994

[18] W. Hong, "Continuum models of stimuli-responsive gels", in S. Li, B. Sun, editors, Advances in Soft Matter Mechanics, pp. 165-196, Springer, Berlin, 2012

[19] W. Hong, X. Zhao, J. Zhou, Z. Suo, "A theory of coupled diffusion and large deformation in polymeric gels", J. Mech. Phys. Solids, Vol. 56, pp. 1779-1793, 2008

[20] W. Hong, Z. Liu, Z. G. Suo, "Inhomogeneous swelling of a gel in equilibrium with a solvent and mechanical load", Int. J. Solids Struct., Vol. 46, pp. 3282-3289, 2009

[21] C. Huet, "Application of variational concepts to size effects", J. Mech. Phys. Solids, Vol. 38, pp. 815–831, 1990

[22] I.-Y. Kim, S.J. Seo, H.S. Moon, M. K. Yoo, In-Y. Park, B.-C. Kim, C. S. Cho, "Chitosan and its derivatives for tissue engineering applications", Biotechnology Advances, Vol. 26, pp 1-21, 2008.

[23] R. Jin, P.J. Dijstra, "Hydrogels for Tissue Engineering Applications", in R. M. Ottenbrite, K. Park, T. Okano, editors, Biomedical applications of hydrogels handbook, pp. 203-225 , Springer, Berlin, 2010

[24] T. Kanit, S. Forest, I. Galliet, V. Mounoury, D. Jeulin, "Determination of the size of the representative volume element for random composites: statistical and numerical approach", Int. J. Solids Struct, Vol. 40, pp. 3647–3679, 2003

[25] D. Lacroix, A. Chateau, M. P. Ginebra, J. A. Planell, "Micro-finite element models of bone tissue engineering scaffold", Biomaterials, Vol. 27, pp. 5326-5334, 2006

[26] H. Li, Smart Hydrogel Modelling, Springer, Berlin, 2009

[27] E. Maire, P. J. Withers, "Quantitative X-ray tomography", International Materials Reviews, Vol. 59, pp. 1-43, 2014

[28] M. A. Meyer, P.-Y. Chen, Biological Materials Science, Cambridge University Press, 2014

[29] H. Omidian, K. Park, "Introduction to hydrogels", in R. M. Ottenbrite, K. Park, T. Okano, editors, Biomedical applications of hydrogels handbook, pp. 1-16, Springer, Berlin, 2010

[30] M. L. Oyen, "Mechanical characterisation of hydrogel materials", International Materials Reviews, Vol. 59, pp. 44-58, 2014

[31] N. A. Peppas, Hydrogels in medicine and pharmacy, vol. 1, CRC Press, Florida, 1987

[32] B. D. Ratner, A. S. Hoffman, F. J. Schoen, J. E. Lemons, Biomaterials Sciences, 3rd edition, App. 8: Properties of Soft Materials by M. C. L. Martins, Elsevier Inc., 2013

[33] B. van Rietbergen, R. Huiskes, F. Eckstein, P. Rüegsegger, "Trabecular Bone Tissue Strains in the Healthy and Osteoporotic Human Femur", J. Bone Miner. Res., Vol. 18, pp. 1781-1788, 2003

[34] H. Shen, L. C. Brinson, "Representative volume element size for porous titanium", J. Mech. Mater. Structures, Vol. 1, pp. 1179–1204, 2006

[35] Simpleware Ltd., Exeter, UK, http://www.simpleware.com, 2014

[36] Suo, http://imechanica.org/node/987, http://imechanica.org/node/538

[37] A. Steinbuchel, editor, Biopolymers, Vols. 5-6, Wiley, Weinheim, 2006

[38] S. K. Wang, J. Li, F. Yao, "Application of Chitosan-Based Biomaterials in Tissue Engineering", in K. Yao, J. Li, F. Yao, Y. Yin, editors, Chitosan-based hydrogels. Functions and Applications, pp. 407-468, SCRC Press, 2012